

# Inverse Design of Passive Photonic Devices with Coupled Electric Dipole Scatterers

Adam Alderton and Prof. Dave Phillips

*Physics Department, University of Exeter*

(Dated: April 2021)

## Abstract

Here presented is the design and implementation of an inverse design algorithm able to optimise the configuration of a set of scattering electric dipoles such that they collectively produce a complex scattering effect. Discussed is the implementation of the design algorithm and its application to optimisation tasks in both two and three dimensions. The algorithm was found to be able to produce intricate scattering behaviour when supplied with hundreds of coupled dipolar scatterers. The design algorithm and its implementation may find utility in computation and communication.

Special thanks to James Capers and Dr. Simon Horsley for their invaluable contribution to the theoretical aspects of this project.

The implementation of the design algorithm in the *C* programming language can be found at [www.github.com/adamalderton](https://www.github.com/adamalderton). All implementation of the inverse design framework discussed is my own, unless otherwise stated.

## CONTENTS

I. Introduction	3
II. The Discrete Dipole Approximation	3
III. The Algorithm for Inverse Design	4
IV. Implementation Considerations	5
A. Finding the Coupling Matrix	5
B. Simplifications	5
C. Fitness Functions	6
V. Input Field Generalisation with the Beam Propagation Method	7
VI. Examples of Applying the Design Algorithm	8
A. Focusing Light in Two Dimensions	8
B. Focusing an Arbitrary Input Field in Two Dimensions	8
C. Multiplexing in Two Dimensions	9
D. Focusing Light in Three Dimensions	10
VII. Suggestions for Future Work	10
A. The Design Algorithm	10
B. Application of the Algorithm	12
C. Physical Realisation of Designed Devices	12
VIII. Relevance, Impact and Long-Term Future Work	12
A. Optical Matrix Computations	12
B. Volume Optics for Spatial Division Multiplexing	13
IX. Conclusion	14
References	14

## I. INTRODUCTION

The design of objects and devices that scatter light is a challenge very relevant to a wide range of fields and interests. Applications lie in the design of metamaterials [1, 2] and imaging through disordered media including biological tissue [3–7]. Methodologies in designing scattering systems also find utility in current research themes relevant to optical communication and computing [6, 8–13]. Purely analytical design of complex scattering systems is challenging and, in general, is not accommodating of any arbitrary desired input-output mapping [1, 2]. Therefore, analogously to the training of a neural network or any other multivariate optimisation process, iterative optimisation algorithms may be applied to be able to inversely design a light manipulating system once given a set of inputs and corresponding desired outputs [14–16].

This work discusses an iterative inverse design algorithm, its implementation, and its application to optimisation problems. Previous work has discussed the

theoretical framework on which the design algorithm is built [2]. The design algorithm considers a large set of discrete coupled scattering electric dipoles which, when iteratively maneuvered to reside in a certain configuration, may produce a collective and complex scattering behaviour close to that conveyed to the algorithm.

The algorithm and its implementation proposed displays advantages over other inverse design algorithms used for similar purposes. Namely, the algorithm can accommodate any means for evaluating the propagation of an input electric field through a scatterer including the *beam propagation method* (BPM). With this, input beams are generalised away from plane waves which other work has been constrained to using [17]. Additionally, the algorithm is built upon the principles of the *discrete dipole approximation* (DDA) which addresses the coupled scattering behaviour of the dipoles [18, 19]. This allows for any weak scattering approximation to be neglected and hence more intricate scattering behaviour can be produced [18]. Furthermore, the design algorithm can function in both two and three dimensions for the design of both surfaces and volumes.

## II. THE DISCRETE DIPOLE APPROXIMATION

The inverse design algorithm employs the principles of the *Discrete Dipole Approximation* (DDA) which is a means to numerically calculate the scattering properties of an object [18, 19]. For dielectric materials, the accuracy of the DDA method can be within a few percent [18].

The DDA method approximates an effectively continuous target as a finite set of discrete electric dipoles with each representing a continuous region of the scattering object [18]. Each of the dipoles gain a polarisation proportional to the electric field of any incident electromagnetic waves on the scattering target [20],

$$\mathbf{P}_j = \alpha_j \mathbf{E}_{\text{in},j}, \quad (1)$$

where  $\alpha_j$  is the polarisability of the  $j^{\text{th}}$  dipole and  $\mathbf{E}_{\text{in},j}$  is the electric field on the location of the  $j^{\text{th}}$  dipole due to the input radiation. Polarisabilities, both scalar and tensor, can be assigned to the dipole as to best represent the scattering behaviour under approximation. For example, the *Clausius-Mosotti* relation [19],

$$\alpha_j = \frac{3d^3}{4\pi} \frac{\epsilon_j - 1}{\epsilon_j + 2} \quad (2)$$

can be used to assign polarisations to the dipoles according to the dielectric function  $\epsilon_j$  of the macroscopic scatterer [18]. Under certain simplifications described and justified in Section IV B and under the considerations of energy conservation, being that the dipoles cannot exhibit gain, a maximum physical polarisability constraint can be derived to be [21],

$$\alpha \leq \frac{6\pi\epsilon_0}{k^3}, \quad (3)$$

where  $k$  is the wavevector of the radiation input into the system.

As the polarised dipoles are effectively a point source for the scattered field, their scattered fields are described by the *Green's function* for the oscillating electric field  $\mathbf{E} = \mathbf{E}_0 e^{ik \cdot \mathbf{r}}$  [20, 22]. That is, the Green's function solution corresponding to the Helmholtz differential operator  $(\nabla^2 + k^2)$  [20],

$$(\nabla^2 + k^2) G(\mathbf{r}, \mathbf{r}') = -\delta(\mathbf{r} - \mathbf{r}'), \quad (4)$$

where  $G(\mathbf{r}, \mathbf{r}')$  is the Green's function solution and  $\delta(\mathbf{r} - \mathbf{r}')$  is the Dirac delta function corresponding to the impulse discontinuous response in the electric field due to the presence of a dipole at exactly the position of the dipole in space [20]. The scalar Green's function that results from equation (4) is [20],

$$G(\mathbf{r}, \mathbf{r}') = \frac{e^{i\mathbf{k} \cdot (\mathbf{r} - \mathbf{r}')}}{|\mathbf{r} - \mathbf{r}'|}, \quad (5)$$

which can be extended beyond this spherical wave solution to capture the dipolar nature of the scattering points [18, 22].

Crucially, the scattered fields emitted from the dipoles, under the discrete dipole approximation, are capable of interacting with other dipoles and capable of effectively scattering again. Therefore, the scattering between all dipoles and all other dipoles is a highly complex system in which the scattering of any one dipole is influenced by all other dipoles. This coupling can be described by a large dense system of  $N$  linear equations [18, 19, 22],

$$\mathbf{E} = \mathbf{A}\mathbf{P}, \quad (6)$$

where  $N$  is the number of dipoles in the set,  $\mathbf{P}$  is a complex vector storing the polarisations of the dipoles and  $\mathbf{E}$  is a complex vector storing the *total* electric fields on the dipoles. That is, the electric fields due to the input radiation and the scattered fields from all other dipoles. The quantity  $\mathbf{A}$  is the *coupling matrix* which holds coefficients describing the propagation of a scattered field from one dipole to another [18]. That is, the matrix element  $\mathbf{A}_{jk}$  propagates the electric field generated by the scattering of dipole  $j$ ,  $\mathbf{E}_j$ , onto dipole  $k$  to contribute to its polarisation  $\mathbf{P}_k$  by equation (1). In the full three dimensional case which takes into the account the dipolar nature of the scatterers, the matrix element  $\mathbf{A}_{jk}$  is a  $3 \times 3$  matrix of the form [18]

$$\mathbf{A}_{jk} = \frac{e^{ikr_{jk}}}{r_{jk}} \times \left[ k^2(\hat{r}_{jk}^2 - \mathbf{I}) + \frac{ikr_{jk} - 1}{r_{jk}^2}(3\hat{r}_{jk}^2 - \mathbf{I}) \right] \quad (7)$$

for  $j \neq k$ , where  $r_{jk} = |\mathbf{r}_j - \mathbf{r}_k|$ ,  $\hat{r}_{jk} = (\mathbf{r}_j - \mathbf{r}_k)/r_{jk}$  and  $\mathbf{I}$  is the  $3 \times 3$  identity matrix. Additionally,  $\mathbf{A}_{jj}$  is defined to be  $\alpha_j^{-1}$  as to prevent a dipole coupling to itself [18]. Notably, the term enclosed by square brackets is the dipole-considering extension to the spherical Green's function solution considered in equation (5).

Once equation (6) has been solved for the polarisations of the dipoles  $\mathbf{P}$ , the total electric field may be evaluated in and around the scatterer by [22],

$$\mathbf{E}(\mathbf{r}) = \mathbf{E}_{\text{in}}(\mathbf{r}) + [\mathbf{A}_{jr} \cdot \mathbf{P}_j](\mathbf{r}), \quad (8)$$

being that the polarisations of the dipoles are propagated onto the point  $\mathbf{r}$  in addition to the presence of the input field.

### III. THE ALGORITHM FOR INVERSE DESIGN

The algorithm for the inverse design of scatterers uses the framework of the DDA to iteratively improve the positions and orientations of a set of dipoles until a desired scattering effect is achieved. The basic steps to this algorithm are as follows:

1. Find the polarisations of the dipoles using equation (6), considering the current positions and orientations of the dipoles.
2. For every dipole in the set, use equation (8) to decide how best to change the position and orientation of the dipole as to most closely match the sought scattering behaviour.
3. Change the positions and orientations of all dipoles using information gained from step 2.
4. Repeat steps 1-3 until the scattering effect of the set of dipoles correlates closely enough with the expected scattering effect passed to the algorithm.

Crucially, the efficiency of the algorithm can be dramatically increased with careful consideration of how, for example, potential new positions of the dipoles are sampled. Without careful consideration, rigorously considering a potential new position would entail temporarily moving the dipole to that position, (expensively) re-solving for the polarisations of the dipoles using equation (6) and finally using equation (8) to once again find the scattering properties of the entire set of the dipoles. A *value-of-merit* describing the correlation between the found scattering behaviour and the wanted scattering behaviour is then calculated and attached to the new position. Should this position have the highest value-of-merit of all the sampled positions for the dipoles, the dipole is then moved to that position.

Clearly, re-solving the large system of equations (equation (6)) for the polarisations of the dipoles for every position considered is very computationally expensive, increasingly so as the size of the set of dipoles increases. However, certain approximations can be leveraged to circumnavigate the need to re-solve the system of equations for all positions considered for all dipoles in the set. If the distances to the positions sampled from the dipoles are small with respect to the inter-dipole separation and are small with respect to the wavelength of the input radiation, then the new coupling matrix for the system with

the temporarily moved dipole  $\mathbf{A}'$  is approximately equal to the coupling matrix of the system before the dipole was temporarily moved  $\mathbf{A}$  [2]. That is, if the dipole is moved only very slightly, the highly non-linear response of the system is linearised such that  $\mathbf{A}' \approx \mathbf{A}$  [2]. A pictorial representation of the short-range position sampling is denoted in FIG. 1.

If the dipoles are moved slightly enough as to hold the approximation  $\mathbf{A}' \approx \mathbf{A}$  then all positions to be sampled for a dipole can be sampled using the already found solution to equation (6),  $\mathbf{A}$ . Critically, this benefit also extends to all other dipoles. That is, all short-range position sampling for all dipoles in the set can, in practice, be carried out with the found  $\mathbf{A}$  matrix as opposed to laboriously finding similar matrices,  $\mathbf{A}'$ , for every dipole in the set [2].

## IV. IMPLEMENTATION CONSIDERATIONS

### A. Finding the Coupling Matrix

Due consideration has to be given as to how to handle the large system of equations describing the coupled scattering between the dipoles, encapsulated in equation (6), such that the optimisation scales reasonably with an increasingly large set of dipoles. Many methods exist to numerically solve a system of equations, both direct and iterative [23]. Consideration also has to be given as to whether the coupling matrix  $\mathbf{A}$  is also be returned. As  $\mathbf{A}$  is independent of the input field  $\mathbf{E}$ , the same  $\mathbf{A}$  can be used for multiple input fields.

LU decomposition with Gaussian elimination is a standard method to directly solve linear systems numerically [23–25]. A solution can be found with approximately  $\frac{2}{3}n^3$  floating point operations where here  $n$  represents the size of the  $n \times n$  matrix which matches the  $n$  dipoles considered under the DDA [25]. A direct inverse to the matrix  $\mathbf{A}$  can be found with LU decomposition with approximately  $\frac{4}{3}n^3$  floating point operations - double that of simply finding a solution [24, 25]. The means by which to find the LU decomposition, Gaussian elimination, can be improved upon with the use of an iterative method such as the conjugate gradient algorithm [18, 23].

While the benefits that iterative solutions provide are appealing, they can be difficult to implement especially for complex vectors and matrices as used in equation (6) [24]. Additionally, the benefits of an iterative solution are most rewarding when a system of equations is sparse which, in general, is not the case for equation (6) [18, 25, 26]. In the interest of obtaining reliable results, LU decomposition with direct Gaussian elimination was used to find the inverse of the coupling matrix  $\mathbf{A}$  such that it can be used for any number of inputs. With the inverse found, the polarisations of the dipoles subject to any input field can be found easily with  $\mathbf{P} = \mathbf{A}^{-1}\mathbf{E}$ . By comparing the number of floating point operations needed to find the inverse as opposed to finding a sin-

gle solution, the strategy of finding the inverse is clearly advantageous when two or more inputs fields are considered.

### B. Simplifications

Various assumptions and simplifications have been used in the development of a program to execute the dipole arrangement optimisation framework. As an introduction, only the positional degree of freedom available to the dipole scatterers is explored. Additionally, the  $3 \times 3$  matrix elements of the coupling matrix  $\mathbf{A}$  have been simplified to scalars such that the dipoles emit spherical waves. Similarly, the polarisability  $\alpha$  of the dipoles is assumed to be scalar. These simplifications have been motivated by computational efficiency and ease of implementation but some have been made for more physical reasons. Namely, the ‘scalar’ dipoles described are more likely to be able to be well represented if physically realised in an experiment [17].

To further increase the computational capabilities of the program, the dipoles are constrained to move on a discrete square grid, be it two or three dimensional. The precision of the grid can be specified such that the grid can closely enough approximate a continuum. The grid constraint allows many integer datatype calculations to be carried out in place of floating point calculations. This expedites calculations of distances and other quantities relevant to the program. However, constraining the dipoles as such can lead to division-by-zero errors if two dipoles are placed exactly on the same lattice point. The program takes measures to prevent this by performing various checks on the state of the grid.

The size of the grid is ensured by the program to be of size  $2^N \times 2^N$  (for the two dimensional case) where  $N$  is an integer. This provides benefits in the storage of grid values but more importantly allows for space efficient *Fast Fourier Transforms* (FFT) [26]. This operation is used throughout the execution of the algorithm. This  $2^N \times 2^N$  grid constraint was implemented with the forethought of potentially using the FFT operation to accelerate the computations needed to find the polarisations of the dipoles, however this technique was not implemented due to this technique not returning the inverse of the coupling matrix,  $\mathbf{A}^{-1}$  [27].

For the prospect a general purpose framework to applicable to a wide range of challenges, the program performs calculations using arbitrary units. That is to say that length scales, input fields, polarisabilities and other parameters available to the program should be carefully considered by the user to be physical and relevant to the particular optimisation task at hand. This however means that the algorithm can be applied to a wide range of length scales for the development of both macroscopic and microscopic scatterers [2, 18]. The polarisabilities given to the dipoles should obey the maximum physical polarisability constraint given by equation (2).

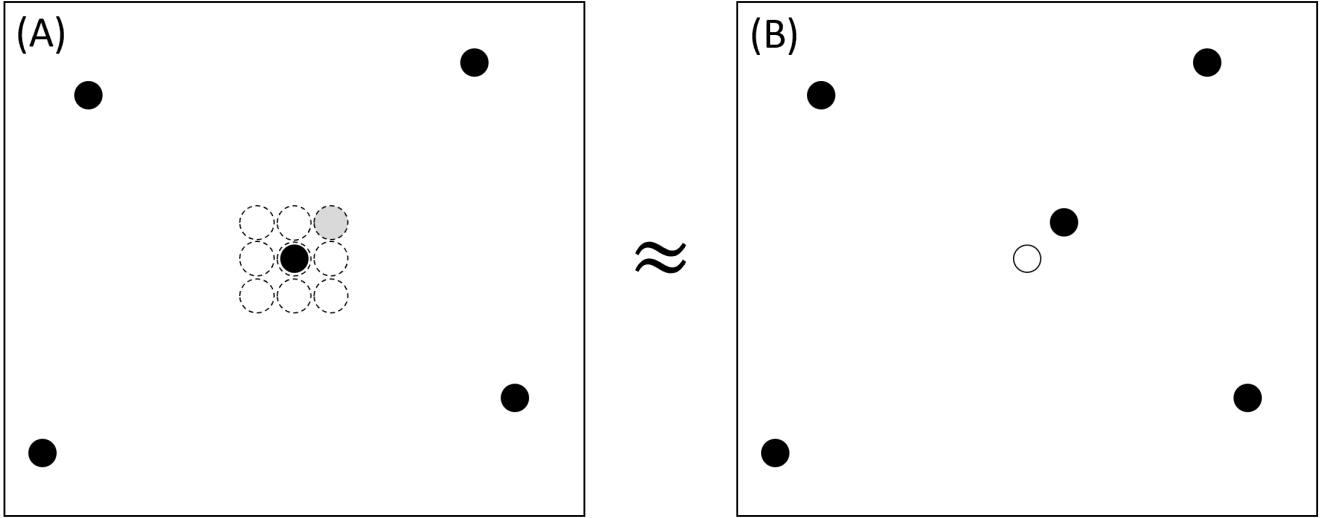


FIG. 1. **(A)**: A set of five dipoles (black circles) is shown. The dipole at the centre of the system is considered to be moved as to alter the scattering properties of the system. Potential new positions close to the dipole are sampled (hollow dotted circles). For example, the position up and to the right may be found to be the most optimal new position for the dipole as highlighted (filled grey). **(B)**: The dipole is moved to the most optimal new position as per step 3 of the algorithm outlined in Section III. The previous position, its position in (A), is shown (hollow solid circle). As the dipole is moved slightly with respect to the other dipoles in the system, the coupling matrices (equation (6)) for the systems are similar,  $\mathbf{A}_B \approx \mathbf{A}_A$ .

### C. Fitness Functions

Step 2 of the optimisation algorithm outlined in Section III mentions the need to decide how best to alter the positions of dipoles and Section III continues to discuss that this is done by assigning values-of-merit to the sampled positions such that the dipole is moved to the position with the highest value of merit. Remaining consistent with the nomenclature of optimisation and machine learning, these ‘values-of-merit’ in optimisation problems are often called *fitnesses* [16]. If an optimisation algorithm is attempting to minimise a quantity, values-of-merit are often called *costs*. Further, iterations of an optimisation algorithm are often named *epochs* [16]. In many gradient descent/ascent optimisation algorithms, the algorithm should endeavour to increase the overall fitness (or decrease the cost) on the execution of every epoch [16]. The design algorithm presented here aims to optimise the correlation between the scattering behaviour of the dipoles and a sought scattering effect. Therefore, the program needs to be able to quantify the correlation (fitness) and be able to quantify how changing the position of a dipole will change (hopefully increase) the overall fitness.

A key constituent of a fitness function within the program is speed as a fitness value must be generated for every position sampled for every dipole. For example, in the three dimensional case, the fitness functions must be called  $27N$  times if positions are sampled around  $N$  dipoles on a  $3 \times 3 \times 3$  grid. The simplest and most intuitive fitness function is a simple dot product between the required electric field to be produced by the system,

and the current electric field produced by the system. While the fitness function benefits greatly from the discretised grid structure discussed in Section IV B and is highly generalised to any input and output fields, it can be argued to be needlessly computationally expensive for simpler tasks such as focusing light to a particular point.

Bespoke, more computationally considerate, fitness functions should be defined on an application-by-application basis as to avoid the default dot product. For example, for the case of focusing a particular input field onto a particular point in space, the total electric field (from the input field *and* scattered from the dipoles) needs to only be evaluated at that point instead of across an entire plane.

For the case of multiplexing two or more input beams such that their transmission can be cast onto separate focus points, clearly more than one focus point is necessary for consideration. Care should then be taken such that the optimisation algorithm does not produce unwanted behaviour. For example, when defining the fitness function to be the sum of the intensities of the focus points,

$$f(\{\mathbf{E}_i\}, \{\mathbf{r}_i\}) = \sum_i |\mathbf{E}_i(\mathbf{r}_i)|, \quad (9)$$

the algorithm was liable to over-committing to one focus point rather than balancing the fitness between them. More reliable results were produced when the algorithm was punished for over-committing. For example, a simple and computationally efficient means to do so was to redefine the fitness function as

$$f(\{\mathbf{E}_i\}, \{\mathbf{r}_i\}) = \sum_i \ln(|\mathbf{E}_i(\mathbf{r}_i)|), \quad (10)$$

such that its logarithmic behaviour induces punishment for over-committing to any one focus point.

Other fitness functions have been implemented in the design algorithm such as the widely used square-difference function. This function actually produces a cost to be minimised but this can easily be converted to a fitness by normalisation and subtraction from 1, for example. The function is defined as [16],

$$f(\{\mathbf{E}_i\}, \{\mathbf{r}_i\}) = \sum_i (\mathbf{E}_i(\mathbf{r}_i) - \mathbf{E}_i^w(\mathbf{r}_i))^2, \quad (11)$$

where  $\mathbf{E}_i^w(\mathbf{r}_i)$  is the electric field value that the ‘wanted’ scattering behaviour would take at the focus point  $\mathbf{r}_i$ . This function and similar functions reward the algorithm should it minimise false-positive responses - pertinent to multiplexing applications [8].

## V. INPUT FIELD GENERALISATION WITH THE BEAM PROPAGATION METHOD

In the process of optimising the arrangement of the dipole scatterers, the algorithm needs to be able to quickly evaluate the total electric field within the area in which the dipoles can be moved. For a time independent plane wave input field, this is easily evaluated by

$$\mathbf{E}(\mathbf{r}) = \mathbf{E}_0 e^{i\mathbf{k}\cdot\mathbf{r}}, \quad (12)$$

where  $\mathbf{E}_0$  is the amplitude of the plane wave. However, the mechanics of the inverse design algorithm are not tied to a particular means of evaluating input fields. Therefore, if other, more general methods are implemented to numerically evaluate the input fields within the scatterer, the inverse design algorithm should be able to accommodate more general input fields.

The *Beam Propagation Method* (BPM) models the propagation of a wavefront through a medium with a refractive index distribution  $n(\mathbf{r})$  [28]. For simplicity, the use of the BPM within the optimisation algorithm is under the assumption that the dipoles move in free space hence  $n(\mathbf{r})$  is simplified to  $n(\mathbf{r}) = 1 \forall \mathbf{r}$ .

The BPM is built on the foundations of Fourier optics, hence Fourier transforms play a large part in the mechanics of the BPM [28]. Given a two dimensional wavefront  $\mathbf{E}(x, y)$  propagating in the  $z$  direction, the wavevector-space representation is found by the two dimensional Fourier transform [28],

$$\tilde{\mathbf{E}}_{z_0}(k_x, k_y) = \mathcal{F}[\mathbf{E}_{z_0}(x, y)](k_x, k_y), \quad (13)$$

where  $z_0$  denotes the initial plane from which the propagation wavefront is evaluated. Given that the wavelength of the (monochromatic) input field is known and that  $k_x$  and  $k_y$  can be retrieved easily from the wavevector-space representation  $\tilde{\mathbf{E}}_{z_0}$ , the unknown  $k_z$  can be evaluated by,

$$k = \frac{2\pi}{\lambda} = \sqrt{k_x^2 + k_y^2 + k_z^2} \quad (14)$$

$$k_z = \sqrt{k^2 - k_x^2 - k_y^2}. \quad (15)$$

More intuitively speaking, the two dimensional Fourier transform described by equation (13) yields the plane wave components  $\tilde{\mathbf{E}}_{z_0}$  that, if combined, would yield the input field  $\mathbf{E}_{z_0}(x, y)$ . With this information, we have deduced  $k_z$  for each plane wave component which then describes how each plane wave component propagates in the  $z$  direction - the direction in which the general wavefront is propagating. Therefore, if we allow each plane wave component to accumulate an appropriate amount of phase as a function of  $k_z$  and a distance  $\Delta z$ , we have propagated the plane wave component in the  $z$  direction by that amount of phase. If we then apply an inverse Fourier transform to the propagated plane waves, we yield the overall propagated field in real space, propagated by  $\Delta z$ . In short, we have used the fact that plane waves are easily evaluated anywhere by equation (12) to propagate the plane wave components of the generally otherwise unevaluable  $\mathbf{E}_{z_0}(x, y)$ . More formally [28],

$$\tilde{\mathbf{E}}_{z_0+\Delta z}(k_x, k_y) = \tilde{\mathbf{E}}_{z_0}(k_x, k_y) e^{-i\sqrt{k^2 - k_x^2 - k_y^2}\Delta z} \quad (16)$$

$$\mathbf{E}_{z_0+\Delta z}(x, y) = \mathcal{F}^{-1}[\tilde{\mathbf{E}}_{z_0+\Delta z}(k_x, k_y)], \quad (17)$$

where  $\mathcal{F}^{-1}$  denotes the inverse Fourier transform. Notably, the propagated beam evaluation has no explicit time dependence nor a particular validity on the propagation distance  $\Delta z$ . Hence, an input beam can be propagated to any plane in a single iteration of the above steps - it does not need to be propagated by a series of short steps in distance, for example [28].

Within the algorithm and otherwise digitally, the discrete two dimensional Fourier transforms can be efficiently found by a series of FFTs [23, 28]. By the *Cooley-Tukey method*, these FFT operations can be carried out *in situ* should the memory allocated for storage be of size  $2^N \times 2^N$  [23, 26]. Therefore, following previous discussion of the advantages of the  $2^N \times 2^N \times 2^N$  lattice on which the dipoles reside, the numerics of the BPM benefit greatly from the constraining discrete grid.

Not only does the BPM agree with the workings of the optimisation algorithm, it also agrees well with the physical world. Namely, by virtue of leveraging Fourier optics, the BPM handles diffraction and interference effects automatically [28].

However, as powerful as it may be, the BPM is still an approximation and is therefore liable to provide unphysical results should its limitations be exceeded [28]. As it is a description of macroscopic light, it can produce unphysical effects when applied to nanophotonic modelling in which, for the general case, formal numerical solutions of Maxwell’s equations should be used instead [20]. Additionally, especially when considering nanophotonics, inaccurate edge effects can arise due to the infinite periodic boundary conditions used by the FFT operations [28].

## VI. EXAMPLES OF APPLYING THE DESIGN ALGORITHM

To demonstrate how the algorithm may work in practice, here it is applied to various design problems in both two and three dimensions. For the wavelengths of light used in all applications, polarisabilities to be assigned to the dipoles were calculated under the constraints of equation (2) such that the simulations produce physical results should the units of length used be on the order of tens of micrometres. Therefore, the wavelengths presented here are on the order of millimetres. As discussed in Section IV, the optimisation program is scale-independent and therefore values of electric field and length below are of arbitrary units of electric field and length respectively.

### A. Focusing Light in Two Dimensions

As a simple test of the algorithm, it was first applied to the challenge of focusing light in two dimensions. The results of the application of the algorithm can be seen in FIG. 2, in which the initial (random) placements of the 150 dipoles are shown alongside the final state of the dipoles after 50 iterations of the steps outline in Section III. As the inverse design algorithm must optimise for the intensity of the electric field on the focus point, a very straightforward fitness function was used: the intensity of the electric field on the focus point.

Interestingly, when in an optimised state, the arrangement of the dipole scatterers appears to be highly ordered and structural. This structure could be described as something analogous to approximately spherical concentric Bragg reflection planes each separated by half the wavelength of the plane wave input field. The half wavelength separation can be understood as the algorithm attempting to obtain the largest contribution to the fitness possible from each dipole. Specifically, as the structures are a half wavelength apart, the structures each correspond to an anti-node of the plane wave propagation. At these anti-nodes, the magnitude of the real part of the electric field is at a maximum hence the dipoles acquire a maximum polarisation in response in agreement with equation (1). With this maximal polarisation, the dipole emits a maximally intense field and hence contributes maximally to the task at hand: maximising the intensity on the focus point. Additionally, remembering that the fields emitted by the dipoles match the wavelength of that of the input field, the field emitted by the dipoles maximally contributes to the polarisation of dipoles in other ‘planes’. Intuitively, the magnitude of the real part of the electric field emitted by a dipole in one of these planar structures is once again maximal once it has propagated by half a wavelength, where, advantageously, the next planar structure of dipoles is situated. Therefore, dipoles in one planar structure gain the maximum polarisation contribution from dipoles in the previous planar

structure, even if the polarisation is out of phase by a factor of  $\pi$ .

### B. Focusing an Arbitrary Input Field in Two Dimensions

To highlight the independence of the design algorithm from the means by which the input field is evaluated throughout the system of dipoles, the BPM was used in conjunction with the design algorithm to address the problem of focusing an effectively arbitrary input field onto a point. An example of the use of the BPM with the design algorithm is presented in FIG. 4. Here, the input field has both a non-trivial spatial dependence and a non-trivial phase dependence, and hence the task of correctly manipulating this input field is complex.

In the example shown in FIG. 4, the dipoles are tasked with maximising the intensity on the focus point hence the fitness function used was simply the intensity on this point. Even when given this simple fitness function, the algorithm must apply correct spatial and phase shifts to the input field as to ensure the most effective constructive interference on the focus point possible. To this end, the dipoles appear to be placed at planes a full wavelength apart, where the variation in placement along these planes can be seen to be imparting the necessary phase and spatial shifts.

Interestingly, for this example, the integer wavelength separation of the structures of dipoles is different to that of the example considered in the case of the simple two dimensional plane wave focusing task, discussed in Section VIA. This is likely due to the smaller wavelength considered here which would result in the dipole structures being highly compacted together should there be one structure for every anti-node of the field in the plane. Hence, perhaps for the minimisation of unwanted and messy coupling, the algorithm arranges the dipoles to reside on further separated structures corresponding to every other anti-node.

The behaviour of the fitness value over the course of the execution of the algorithm when provided this example is displayed in FIG. 3. Interestingly, the fitness reaches a maximum value at the 76<sup>th</sup> iteration as opposed to the final iteration, the 100<sup>th</sup>. This indicates that, clearly, the system cannot be significantly optimised further beyond the configuration at the 76<sup>th</sup> iteration. More interestingly, the question could be asked as to why the fitness reduces slightly past the 76<sup>th</sup> iteration, rather than plateauing at this maximal fitness. Potentially, a number of effects may be exerting their influence here.

One effect that is likely to be significant is that the precision of the discrete grid on which the dipoles are constrained is not sufficient for further optimisation. That is, the optimum position of a dipole resulting from the next iteration can no longer be approximated to lie on the constraining grid - the positions of the dipoles must be freed to the continuum for further optimisation. This concept

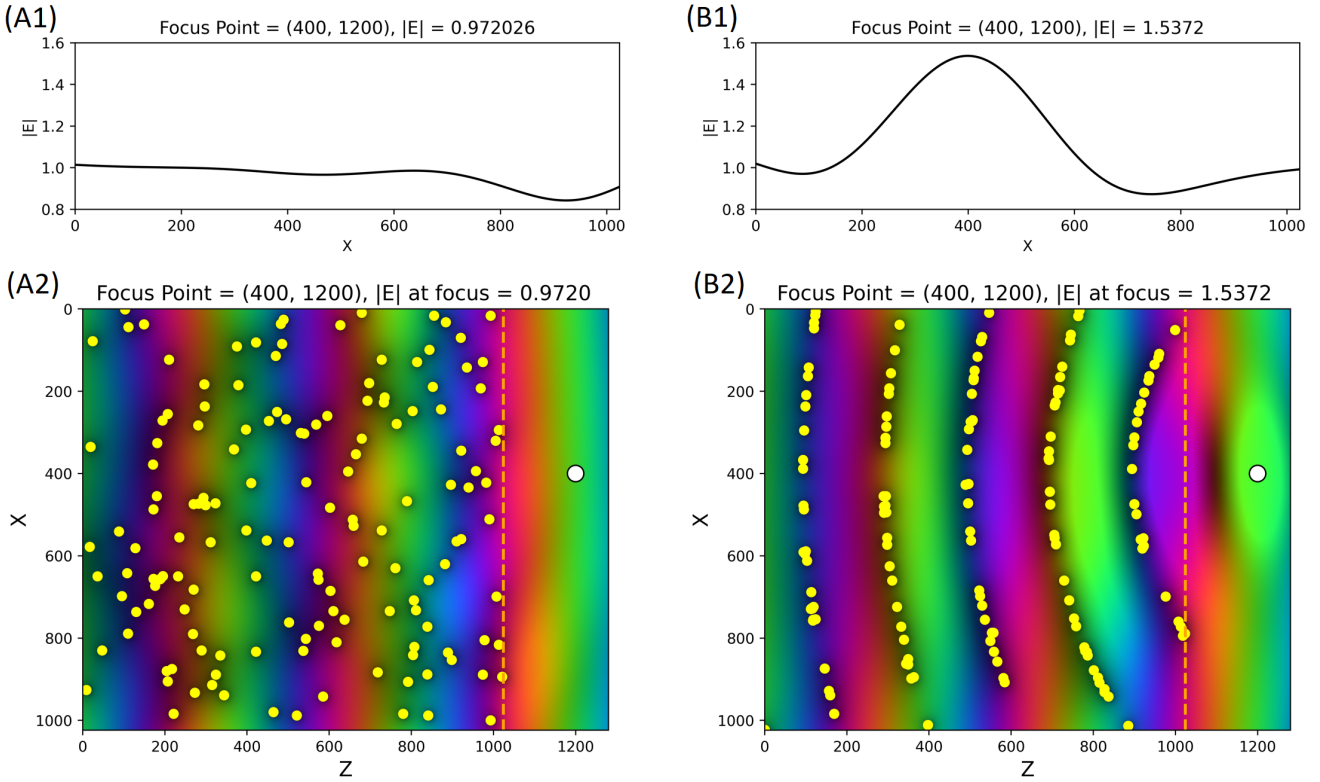


FIG. 2. The results of the inverse design algorithm applied to a system of 150 dipoles instructed to focus an incoming plane wave of amplitude  $|E| = 1$  (arbitrary units). The input plane wave of wavelength 400 (arbitrary units) is incident on the system from the negative  $z$  direction and is focused onto the point  $(x = 400, z = 1200)$ . **(A1)**: The profile of the intensity  $|E|$  at the plane  $z = 1200$  in (A2), matching that of the focus point. The profile spans the width of the scatterer in the  $x$  dimension. **(A2)**: The two dimensional scattering system containing 150 randomly placed scattering dipoles (yellow points). The dipoles are constrained to a square lattice of size  $1024 \times 1024$ . The amplitude and phase of the electric field is represented by brightness and colour respectively. **(B1)**: The intensity profile corresponding to the plane  $z = 1200$  in (B2). A peak in intensity is shown at the focus point  $x = 400$ . **(B2)**: The arrangement of the 150 dipoles in (A2) after 50 iterations of the inverse design algorithm. The dipoles form a highly ordered multilayered spherical planar structure in efforts to maximise the intensity on the focus spot demonstrates a 53.7% increase over input field intensity - an increase of 0.36% per dipole.

may be compared directly to the concept of *learning rate* within the context of machine learning and other optimisation processes. Learning rate is the quantity by which the system is improved upon when applying gradient descent techniques [16]. Specifically, if the system is too far improved in one iteration, the configuration may ‘jump’ over minima as opposed to exploring them especially if the parameter space could be considered to be ‘rough’ [16]. The analogue of learning rate in the case of the inverse design algorithm presented is the separation of the grid points. Intuitively, if the grid spacing is too large, the dipoles may ‘overshoot’ their most optimum position.

Another effect that may be causing the gradual reduction in fitness past the maximum may be that the coupling matrix approximation loses validity when a highly optimised state is reached. This approximation, that the same coupling matrix  $\mathbf{A}$  can be used throughout an iteration was discussed at length in Section III. It relies

on the movement of the dipoles during an iteration to be small when compared to the inter-dipole separation. Clearly, for the results displayed in FIG. 4 and other results presented here, the dipoles can be inclined to form tightly packed structures which certainly break the large separation approximation.

### C. Multiplexing in Two Dimensions

The capability of the algorithm to perform optimisations for complex tasks, such as multiplexing two input beams, is demonstrated here. That is, the arrangement of dipoles needs to able to focus two different incoming plane waves (of different incident angles) onto two separate points, and minimise the possibility of obtaining a false-positive result if the intensity on the focus points were to be measured. The results of the algorithm ap-

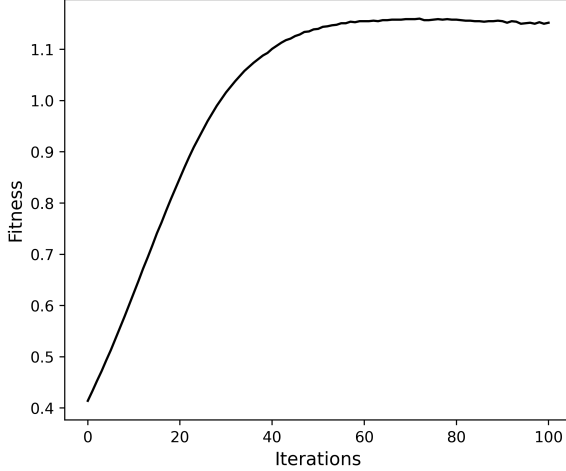


FIG. 3. The value of the overall fitness returned by the fitness function for the optimisation process discussed in Section VI B, concerning the design of a scattering system able to focus a non-trivial input field onto a point. The fitness function used was simply the value of the intensity on the focus point. Over the course of the optimisation, the fitness reaches a maximum value of 1.1586 on the 76<sup>th</sup> iteration, before tapering slowly to a final, lower, value of 1.1577 on the 100<sup>th</sup> iteration.

plied to this concept are presented in FIG. 5.

Here, the choice of fitness function was key. A modified difference-of-squares function was used using concepts outlined by equations (10) and (11). That is, the square difference in the value wanted and the current value for intensity, at both the points, was square rooted and passed to the natural logarithm function as,

$$f(\{\mathbf{E}_i\}, \{\mathbf{r}_i\}) = \sum_i \ln(|\mathbf{E}_i(\mathbf{r}_i)| - |\mathbf{E}_i^w(\mathbf{r}_i)|), \quad (18)$$

where the symbols match those given in equation (11). By setting the ‘wanted’ intensity value on the focus point of the input beam *not* currently under consideration to a low value, the algorithm is punished should the intensity increase on the unwanted focus point. Therefore, false-positive signals are minimised. The use of the natural log function ensures that the algorithm is punished for over-committing to focusing one input field.

The reduction of the false-positive signals as a result of the use of the fitness function in equation (18) can be observed in the intensity profiles presented in FIG. 5. For the two focus points ( $x = 800, z = 1200$ ) and ( $x = 200, z = 1200$ ), the intensity is correctly minimal on or near to the ‘secondary’ focus point when the intensity should be maximal on the ‘primary’ focus point.

The behaviour of the field propagating through the set of dipoles in this example is interesting as the arrangement of dipoles appears to be exhibiting highly differing collective polarisations for one input and for the other.

Clearly, to give radically different output intensity profiles when receptive to the two separate inputs, the collective response of the system of dipoles should be radically different and organised especially as to ensure the minimisation of false-positive responses.

#### D. Focusing Light in Three Dimensions

To exhibit the applicability of the algorithm to the design of scattering volumes, it was applied to the task of focusing a three dimensional plane wave onto a point. The results of the inverse design algorithm applied to 80 dipoles confined to a volume are shown in FIG. 6. In agreement with the challenge of focusing a two dimensional plane wave as visited in Section VI A, the dipoles form approximately equidistant planar structures such that their separation is approximately equal to half of the wavelength of the plane wave input field. That is, one structure per anti-node. Conjecture as to why these structures form has been discussed in Section VI A.

Notably, and perhaps unsurprisingly, the time needed to apply the optimisation algorithm in three dimensions (approximately 60 minutes for 100 dipoles) is much greater than the two dimensional case (approximately 5 minutes for 100 dipoles). This is largely due to the need to calculate two dimensional discrete Fourier transforms to propagate the input beam in the three dimensional case. Additionally,  $3^3 \times N$  positions must be sampled per iteration in the three dimensional case compared to  $3^2 \times N$  in the two dimensional case, where  $N$  is the number of dipoles. However, for relatively simple tasks such as focusing a three dimensional plane wave, simpler means were used to evaluate the wave throughout the volume. The beam propagation method was used in the example presented in FIG. 6 for completeness but identical results were obtained by evaluating  $e^{ik\mathbf{r}}$  throughout the structure instead. Additionally, similar results were also obtained when using an emitting dipole as the source field under the condition that the emitting dipole was sufficiently distanced from the scattering volume such that its emitted spherical field closely approximates a plane wave throughout the volume. When using these simpler methods for evaluating the plane wave input throughout the volume, the average execution time reduced from approximately 60 minutes to approximately 10 minutes.

## VII. SUGGESTIONS FOR FUTURE WORK

### A. The Design Algorithm

Concerning the further development of the design algorithm, a number of simplifications and assumptions could be improved upon or overwritten explicitly. For example, the degree of freedom representing the orientation of the dipole in space could be explored alongside the positional degree of freedom. More exotic polarisabilities could be

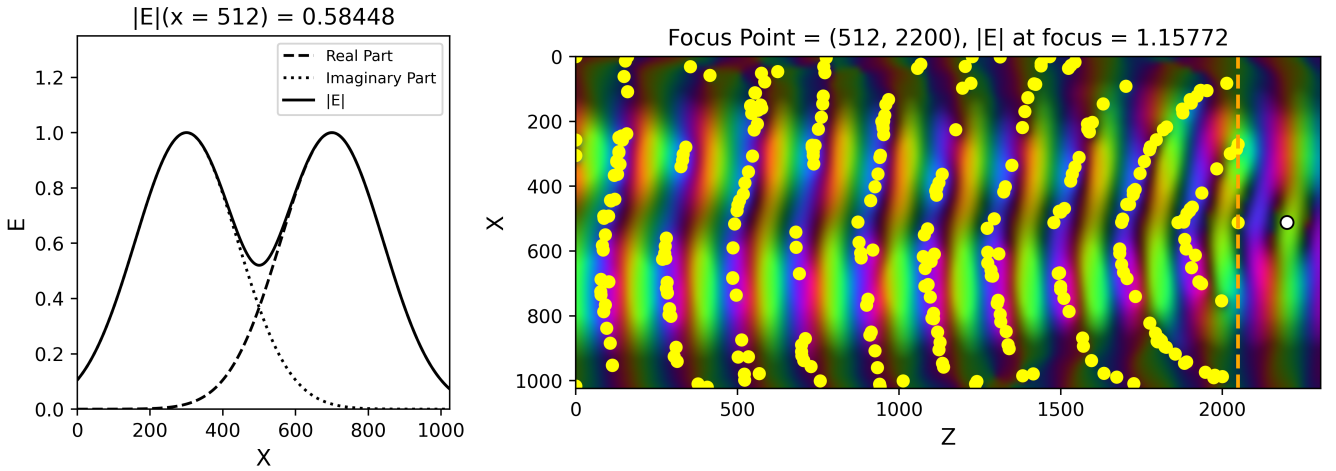


FIG. 4. The results of the inverse design algorithm applied to the challenge of focusing a non-trivial input field onto the point  $(x = 512, z = 2200)$ , with the use of 300 dipoles. (left): The profile of the input beam. It constitutes two Gaussian beams out of phase by a factor of  $\frac{\pi}{2}$  such that one beam is purely real at  $z = 0$  and the other is purely imaginary at  $z = 0$ . The intensity profile of the combined beams is therefore a twin peaked Gaussian. (right): The placements of 300 initially randomly placed dipoles (yellow points) subject to 100 iterations of the optimisation algorithm. They are shown amongst the electric field due to the input field (wavelength of 200 arbitrary units) and the scattering of the dipoles, with colour and brightness corresponding to phase and amplitude respectively. The black and white marker indicates the focus point. The focus point has an intensity 98.1% larger than that of the same point in the original input beam.

explored outside of isotropically applying a scalar polarisability to the dipoles.

In regards to the actual implementation of the algorithm, much time could be usefully spent altering or improving some aspects. The limiting resource to the algorithm is currently processing power and speed. Therefore, the implementation would greatly benefit in trading some compute resources for memory consumption. For example, instead of calculating propagation by the beam propagation every time an electric field value is needed, all field values could be calculated throughout the structure at the start of the iteration and subsequently stored therefore avoiding duplicate calculations. The constraining grid technique used throughout this work would ensure that no field interpolation would be necessary to calculate or store.

Further optimisations could be made to the process behind how the dipole coupling system of equations is solved. Clearly, these optimisations would yield the most reward for increasingly large systems of dipoles. As an example, setting the coupling coefficient for distant dipoles to be zero such that sparse matrix solutions could be used would be highly beneficial. Additionally, fast Fourier transforms may be used to solve these equations very efficiently should the dipoles be constrained to the discrete grid discussed, as touched upon in Section IV B

[27]. This technique does not return the coupling matrix  $\mathbf{A}$  and hence would only be useful in the case of optimising for a single input field [27].

As discussed throughout, the implementation would of course benefit from parallelisation as currently all computations are carried out serially. Specifically, finding the coupling matrix  $\mathbf{A}$  could be carried out across multiple threads. Furthermore, the optimisation of a dipole within an iteration is entirely independent of all other dipoles (due to the constant coupling matrix approximation) and hence could be easily parallelised. Finally, the two dimensional Fourier transform necessary in the three dimensional beam propagation method could also be parallelised.

Finally, other optimisation techniques could be used to complement the central gradient descent technique. The sole use of this technique severely limits the exploration of the parameter space, as, clearly, it simply converges onto the nearest significant optimised state. The technique known as *simulated annealing* amongst others is commonly used to quickly search large parameter spaces [16]. This technique was preliminarily explored in this work and did show promise of being an interesting avenue to explore.

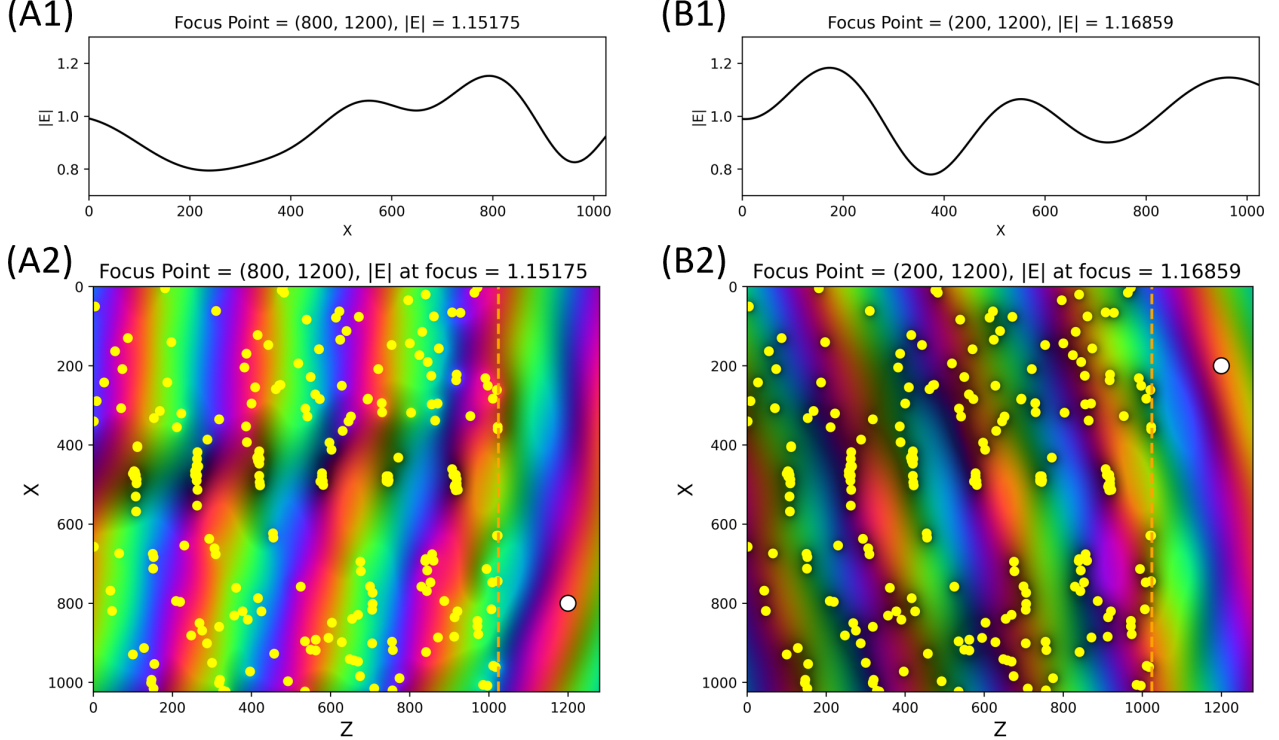


FIG. 5. The results of the inverse design algorithm applied to the challenge of multiplexing two simple input beams. 250 initially randomly placed dipoles (yellow points) are used to focus two incoming plane waves incident on the system from differing angles. The two plane wave inputs  $A$  and  $B$ , both of intensity 1.0 (arbitrary units) and wavelength 300 (arbitrary units), are described by (A1), (A2) and by (B1), (B2) respectively. The plane waves are focused by the same arrangement of dipoles to yield intensity increases of 15.1% and 16.9% respectively on their respective focus points. (A1): The intensity profile of the electric field at the plane  $z = 1200$  due to the input of plane wave  $A$ . (A2): The arrangement of dipoles amongst the electric field due to plane wave  $A$ , with phase and amplitude indicated by colour and brightness respectively. The focus point ( $x = 800, z = 1200$ ) is denoted by the black and white marker. (B1): The intensity profile of the electric field at the plane  $z = 1200$  due to the input of plane wave  $B$ . (B2): The arrangement of dipoles amongst the electric field due to plane wave  $B$  with phase and amplitude represented by colour and brightness respectively. The focus point ( $x = 200, z = 1200$ ) is indicated by the black and white marker.

### B. Application of the Algorithm

The main challenge concerning the second vein of further work, the application of the algorithm, is the use of many more dipoles. This vein complements the former as more dipoles can be included and hence more degrees of freedom can be explored for optimised states. With more dipoles, more complex scattering behaviour should be able to be designed, especially in three dimensions. Further discussion as to how the algorithm may be applied in future is outlined in Section VIII.

### C. Physical Realisation of Designed Devices

The final vein of future work addresses the task of realising a designed scatterer in a lab setting. A method by which to do this could be by using a femtosecond

laser to directly write dipole-like scatterers in a volume of glass [29]. The laser could be used to concentrate large amounts of energy in small volumes of the glass, causing small bubbles of gas to form [29]. The bubbles formed would have a refractive index largely different to that of the glass around them and would hence scatter light perhaps similarly to the dipoles considered in this work [29].

## VIII. RELEVANCE, IMPACT AND LONG-TERM FUTURE WORK

### A. Optical Matrix Computations

Large and complex scattering systems and their subsequent design have very recently found strong applicability in the optical computing space [9–13]. This ap-

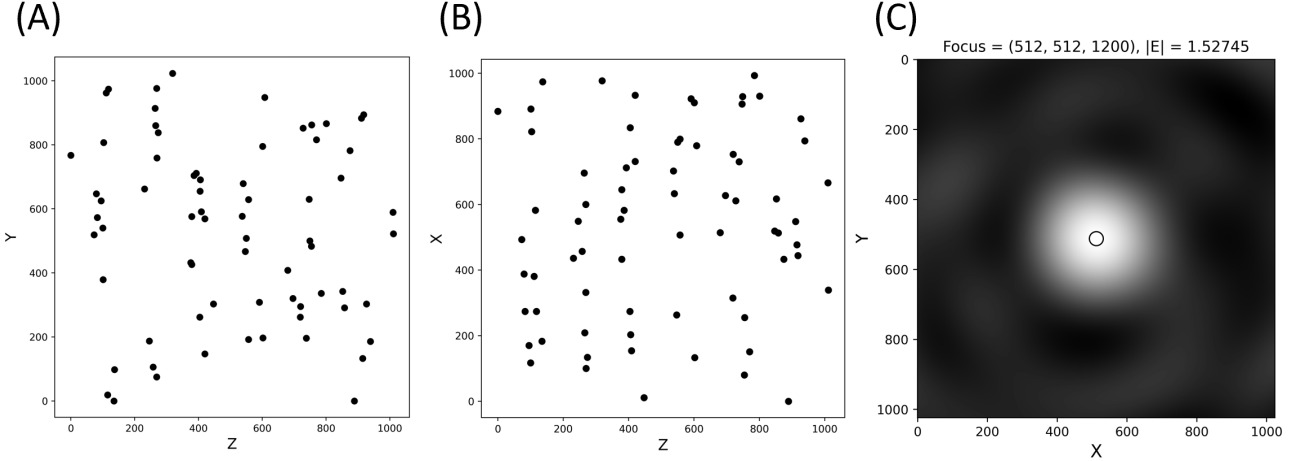


FIG. 6. The results of the inverse design algorithm when applied to the task of focusing a three dimensional plane wave onto a point in a two dimensional plane. 80 dipoles are confined in a cubic region of space of dimensions  $1024 \times 1024 \times 1024$ . The input plane wave is incident on the system of dipoles from the negative  $z$  direction and propagates in the positive  $z$  direction with a wavelength of 300 (arbitrary units). (A) and (B): The placements of the initially randomly placed dipoles after 100 iterations of the inverse design algorithm. These figures show the projections of the positions along the  $z-y$  plane and the  $z-x$  plane respectively. The dipoles appear to congregate on planes separated by half the wavelength of the incoming plane wave. (C): The intensity profile of the electric field across the  $x-y$  plane at  $z = 1200$  which lies outside of the confining volume. The focus point is indicated by the black and white marker. For this arrangement of dipoles, the intensity on the focus point is 52.7% larger than that of the incoming plane wave.

plication is underpinned by the use of a quantity known as the *transmission matrix*. This is an experimentally measurable quantity that fully describes the scattering properties of the system - avoiding the need to study the incredibly complex microscopic details [3, 4]. This quantity and its study stems from the idea of inverting this matrix as to be able to image through complex media such as living tissue [4–7].

As the transmission matrix is a matrix, it may be considered to be applied to matrix-vector multiplications. That is, if a vector of data to be computed is represented as an electric field in the same basis as the basis in which the transmission matrix is defined, the transmission matrix will operate on this data as the field is scattered to produce a resulting vector of data - completely in parallel [6, 10]. Success has been found in this idea with spatial light modulators (SLMs) used to operate on the data, with computation times yielding results two to three orders of magnitude faster than in the electronic case [9]. However, computations with SLMs are difficult to scale to large matrices [9]. Commercial success has been found in using large complex scatterers, and their corresponding transmission matrices, in the field of machine learning [9–13]. Large random matrix computations, pertinent to machine learning under random matrix theory, can be carried out extremely quickly by an essentially random scatterer and hence vastly outperform their electronic counterparts [10].

Algorithms and frameworks such as that discussed in this work may be able to design a large scattering system once provided with an arbitrary transmission matrix to

design around. Should this be possible, potentially extremely large scatterers with extremely large transmission matrices could be designed and hence used in the optical computing space. As a matrix describes a linear operation, more interesting scattering behaviour could be designed around including a linear optical ‘perceptron’ - a primitive linear optical neural network [16].

## B. Volume Optics for Spatial Division Multiplexing

Optical fibre communication has largely saturated the capabilities of multiplexing in time, frequency, polarisation and phase [8]. Now, the industry is beginning to explore space as a degree of freedom within which to multiplex data channels [8, 30]. Many effective techniques are available for spatially multiplexing data channels before transmission including the use of photonic lanterns and multi-plane light conversion [14, 31].

Similar techniques can often be applied to demultiplexing the transmitted channels [8]. However, challenges arise when the channels must be demultiplexed after traversing a comparatively long distance. Multi-mode and few-mode fibres are highly scattering systems and hence can be described by a transmission matrix, a quantity discussed in Section VIII A. The output distorted beam, the *speckle pattern*, should be a linear combination of the speckle patterns produced by the individual spatial modes passed through the scattering fibres [15]. Hence, machine learning techniques have been applied to these speckle patterns as to *actively* demultiplex

the output signal [15, 32–34]. However, the application of machine learning suffers from conversion loss and sub-sampling and is of course active whereas, for any realistic system, the demultiplexing device should be passive [8].

This work and its discussion could lead to the production of passive optical devices to replace the active neural network classifiers. Intuitively, such a device may have a transmission matrix equal to the inverse of the transmission matrix of the scattering fibre, therefore passively and seamlessly recovering the original unscrambled signals. The three dimensional capabilities of the design algorithm described here also has a role to play as a volumetric optical device would be able to overcome the upper limit of the multiplexing abilities of two dimensional devices [17, 35].

## IX. CONCLUSION

This work has presented an implementation and discussion of an inverse design algorithm able to iteratively improve the positions of a set of dipoles such they produce a collective scattering behaviour. Here, this implementation has been applied to two and three dimensional problems as well as challenges requiring arbitrary input field propagation.

The algorithm and its implementation was able to produce intricate structures when meeting design specifications including planar structures to leverage maximal resonant re-scattering and structures able to exert phase and spatial shifts simultaneously.

This implementation and its handling of arbitrary input fields may aid in the design of large and arbitrarily complex scatterers able to perform linear transformations and computations in the parallel and energy-efficient optical domain.

- 
- [1] W. Huang, Z. Wei, B. Tan, S. Yin and W. Zhang, *Journal of Physics D: Applied Physics* **54**, 13 (2021).
  - [2] J. R. Capers, S. J. Boyes, A. P. Hibbins and S. A. R. Horsley, *ArXiv Pre-Print arXiv:2011.13274*, (2020).
  - [3] I. M. Vellekoop and A. P. Mosk, *Physical Review Letters* **101**, 120601 (2008).
  - [4] A. P. Mosk, Á. Lagendijk, G. Lerosey and M. Fink, *Nature Photonics* **6**, 283 (2012).
  - [5] S. M. Popoff, G. Lerosey, R. Carminati, M. Fink, A. C. Boccara and S. Gigan, *Physical Review Letters* **104**, 100601 (2010).
  - [6] S. Rotter and S. Gigan, *Reviews of Modern Physics* **89**, 015005 (2017).
  - [7] J. Bertolotti, E. G. van Putten, C. Blum, A. Lagendijk, W. L. Vos and A. P. Mosk, *Nature* **491**, 232 (2012).
  - [8] D. J. Richardson, J. M. Fini and L. E. Nelson, *Nature Photonics* **7**, 354 (2013).
  - [9] H. J. Caulfield and S. Dolev, *Nature Photonics* **4**, 261 (2010).
  - [10] J. Dong, M. Rafayelyan, F. Krzakala and S. Gigan, *IEEE Journal of Selected Topics in Quantum Electronics* **26**, 1 (2019).
  - [11] A. Saade, F. Caltagirone, I. Carron, L. Daudet, A. Dremeau, S. Gigan and F. Krzakala, *2016 IEEE International Conference on Acoustics, Speech and Signal Processing*, 6215 (2016).
  - [12] M. Rafayelyan, J. Dong, Y. Tan, F. Krzakala and S. Gigan, *Physical Review X* **10**, 041037 (2020).
  - [13] R. Ohana, J. Walker, J. Dong, S. Marmin, F. Krzakala, M. Filippone and L. Daudet, *2020 IEEE International Conference on Acoustics, Speech and Signal Processing*, 9292 (2020).
  - [14] G. Labroille, B. Denolle, P. Jian, P. Genevaux, N. Treps and J. Morizur, *Optics Express* **22**, 13 (2014).
  - [15] J. Pauwels, G. Van der Sande and G. Verschaffelt, *Scientific Reports* **9**, 17597 (2019).
  - [16] C. M. Bishop, *Pattern Recognition and Machine Learning*, (Springer, New York, 2016).
  - [17] T. D. Gerke and R. Piestun, *Nature Photonics* **4**, 188 (2010).
  - [18] B. T. Draine and P. J. Flatau, *Journal of the Optical Society of America A* **11**, 4 (1994).
  - [19] E. M. Purcell and C. R. Pennypacker, *The Astrophysical Journal* **186**, 705 (1973).
  - [20] D. J. Griffiths, *An Introduction to Electrodynamics*, (Cambridge University Press, Cambridge 1999).
  - [21] A. B. Evlyukhin, C. Reinhardt, A. Seidel, B. S. Luk'yanchuk, and B. N. Chichkov, *Physical Review B* **82**, 045404 (2010).
  - [22] G. H. Goedcke and S. G. O'Brien, *Applied Optics* **27**, 12 (1988).
  - [23] W. H. Press, S. A. Teukolsky, W. T. Vetterling, and B. P. Flannery, *Numerical Recipes in C*, (Cambridge University Press, Cambridge, 1992).
  - [24] S. C. Chapra and R. P. Canale, *Numerical Methods for Engineers*, (McGraw-Hill, New York, 2015).
  - [25] L. N. Trefethen and D. Bau, *Numerical Linear Algebra*, (Society for Industrial and Applied Mathematics, Philadelphia, 1997).
  - [26] M. Galassi, J. Davies, J. Theiler, B. Gough, G. Jungman, P. Alken, M. Booth, F. Rossi and R. Ulerich, *GNU Scientific Library 2.6 Reference Manual*, (2019).
  - [27] J. J. Goodman, B. T. Draine and P. J. Flatau, *Optics Letters* **16**, 15 (1991).
  - [28] K. Okamoto, *Fundamentals of Optical Waveguides*, (Academic Press, Amsterdam, 2011).
  - [29] Y. Bellouard and M. Hongler, *Optics Express* **19**, 7 (2011).
  - [30] R. G. H. van Uden, R. A. Corres, E. A. Lopez, F. M. Huijskens, C. Xia, G. Li, A. Schulgen, H. de Waardt, A. M. J. Koonen and C. M. Okonkwo, *Nature Photonics* **8**, 865 (2014).
  - [31] A. M. Velázquez-Benítez, J. E. Antonio-López, N. K. Fontaine, R. Ryf, H. Chen, J. Hernández-Cordero, P. Sillard, C. Okonkwo, S. G. Leon-Saval and R. Amezcua-Correa, *Scientific Reports* **8**, 8897 (2018).

- [32] B. Rahmanu, D. Loterie, G. Konstantinou, D. Psaltis and C. Moser, *Light: Science and Applications*, **7**, 69 (2018).
- [33] U. Kürüm, P. R. Wiecha, R. French and O. L. Muskens, *Optics Express*, **27**, 15 (2019).
- [34] J. Zhao, X. Ji, M. Zhang, X. Wang, Z. Chen, Y. Zhang and J. Pu, *JPhys Photonics* **3**, 015003 (2021).
- [35] R. Piestun and C. M. de Sterke, *Optics Letters* **34**, 6, (2009).